Applied Physics Letters ARTICLE pubs.aip.org/aip/apl

Stabilizing perpendicular magnetic anisotropy with strong exchange bias in PtMn/Co by magneto-ionics

Cite as: Appl. Phys. Lett. **124**, 232403 (2024); doi: 10.1063/5.0213731
Submitted: 12 April 2024 · Accepted: 27 May 2024 ·
Published Online: 5 June 2024

Beatrice Bednarz,[1,a] Maria-Andromachi Syskaki,[1,2] Rohit Pachat,[3] Leon Prädel,[4] Martin Wortmann,[5] Timo Kuschel,[5] Shimpei Ono,[6] Mathias Kläui,[1] Liza Herrera Diez,[3] and Gerhard Jakob[1,a]

AFFILIATIONS

[1]Institute of Physics, Johannes Gutenberg University Mainz, Staudingerweg 7, 55128 Mainz, Germany
[2]Singulus Technologies AG, Hanauer Landstraße 103, 63796 Kahl am Main, Germany
[3]Centre de Nanosciences et de Nanotechnologies, CNRS, Université Paris-Saclay, 10 Boulevard Thomas Gobert, 91120 Palaiseau, France
[4]Max Planck Institute for Polymer Research, Ackermannweg 10, 55128 Mainz, Germany
[5]Faculty of Physics, Bielefeld University, Universitätsstraße 25, 33615 Bielefeld, Germany
[6]Central Research Institute of Electric Power Industry, Yokosuka, Kanagawa 240-0196, Japan

[a]**Authors to whom correspondence should be addressed:** bbednarz@uni-mainz.de and jakob@uni-mainz.de

ABSTRACT

Electric field control of magnetic properties offers a broad and promising toolbox for enabling ultra-low power electronics. A key challenge with high technological relevance is to master the interplay between the magnetic anisotropy of a ferromagnet and the exchange coupling to an adjacent antiferromagnet. Here, we demonstrate that magneto-ionic gating can be used to achieve a very stable out-of-plane (OOP) oriented magnetization with strong exchange bias in samples with as-deposited preferred in-plane (IP) magnetization. We show that the perpendicular interfacial anisotropy can be increased by more than a factor 2 in the stack Ta/Pt/PtMn/Co/HfO_2 by applying −2.5 V gate voltage over 3 nm HfO_2, causing a reorientation of the magnetization from IP to OOP with a strong OOP exchange bias of more than 50 mT. Comparing two thicknesses of PtMn, we identify a notable trade-off: while thicker PtMn yields a significantly larger exchange bias, it also results in a slower response to ionic liquid gating within the accessible gate voltage window. These results pave the way for post-deposition electrical tailoring of magnetic anisotropy and exchange bias in samples requiring significant exchange bias.

In view of the climate crisis and the rapidly growing power consumption of information and communication technology, more energy-efficient data storage and processing are needed.[1,2] In that respect, voltage control of magnetic properties is one of the central approaches with high potential for ultralow-power data storage as well as energy-efficient hardware for dissipative and neuromorphic computing.[3–8] Particularly large magneto-electric effects of over 7000 fJ/Vm, calculated as the change in magnetic anisotropy divided by the applied electric field, can be obtained with magneto-ionics using the electric field induced motion of mobile ions.[9] Magneto-ionics has been shown to allow for low-power switching of magnetization,[10] manipulation of the exchange bias (EB),[11,12] and the Dzyaloshinskii–Moriya interaction[13] as well as the control of domain wall nucleation and motion.[14,15]

EB is fundamental to many technological applications. It describes the pinning of the magnetization of a ferromagnetic (FM) material by the uncompensated magnetic moments of an adjacent antiferromagnet (AFM), causing a shift of the magnetization curve along the magnetic field direction. Its applications range from pinning the reference layer in spin valves for magnetic memories, sensors, and spintronic devices,[16] to replacing the auxiliary magnetic field and allowing for field-free switching of magnetization,[17] to imprinting domain patterns for magnetophoretic applications.[18] So far, research on the control of EB has focused on manipulation of the EB in samples with a fixed magnetization direction.[5,11,12,19,20] This was achieved by transfer of different ions, e.g., O,[21] H,[12] Li,[22] as well as N.[23] Different material systems were shown to allow for the manipulation of EB, ranging from systems with the AFM on top[19] or below[11] the FM and

with insulating[11] as well as metallic AFMs.[19] However, so far, a demonstration of the possibility to rotate the magnetization from an in-plane (IP) to an out-of-plane (OOP) state while retaining a strong EB is still missing. This would be highly desirable, e.g., to program 3D magnetization sensors for which one part of the sensor needs to have IP magnetization and another part OOP magnetization.

In this paper, we investigated the effect of magneto-ionic gating on EB between platinum-manganese (PtMn) and cobalt (Co) thin films. We applied the ionic liquid gating technique, enabling large-area gating with simple sample fabrication and applicability to a wide range of materials. In the as-grown state, the system exhibits IP magnetization. By gating, we demonstrate the rotation of the magnetization into a nonvolatile state with OOP magnetization and OOP EB. Notably, this OOP state is the energetically favorable one once it is reached. To better understand the influence of the AFM layer thickness, we compare two stacks with different PtMn thicknesses. We show that there is a trade-off between the strength of the EB in the final state and the speed of the gating process within the accessible gate voltage window until substantial oxidation of the Co. In thinner (8 nm) samples, the magnetization can be rotated faster while thicker (20 nm) samples show a stronger EB.

We have studied magnetic stacks with the composition Ta (5 nm)/Pt (3 nm)/PtMn (t)/Co (0.9 nm)/HfO_2 (3 nm) deposited on thermally oxidized Si/SiO_2 substrates, with two thicknesses of PtMn ($t = 8$ and 20 nm) [Fig. 1(a)]. Co was chosen as the FM material because it can have strong perpendicular magnetic anisotropy (PMA). PtMn, a metallic AFM, is commonly used in the industry because of its ability to provide a strong EB with high thermal stability.[24,25] The seed layers Ta and Pt provide a smooth surface and matching lattice constant for an optimized growth of PtMn. Co was capped with HfO_2, which serves as a donor for mobile oxygen species. It is a high-κ dielectric with large technological relevance[26] and allows for high ion-mobility at low voltages. To ensure very high sample quality, the stacks were sputtered in an industrial Singulus Rotaris magnetron sputtering tool at room temperature. As an isolating layer, HfO_2 was sputtered using RF voltages. The further layers of the stack are metallic and sputtered by DC voltages. To move the mobile oxygen species inside the HfO_2, a droplet of the ionic liquid 1-ethyl-3-methylimidazolium-bis (trifluoromethylsulfonyl)-imide ($[EMIM]^+$ $[TFSI]^-$) was added on the sample surface, and a glass plate coated with indium tin oxide (ITO) was placed on top. The gate voltage was then applied from the ITO electrode across the ionic liquid and HfO_2 to the metallic layers at the bottom of the material stack, which were contacted by wire bonding [Fig. 1(a)]. In this way, a sample area of approximately $5 \times 5\ mm^2$ was gated.

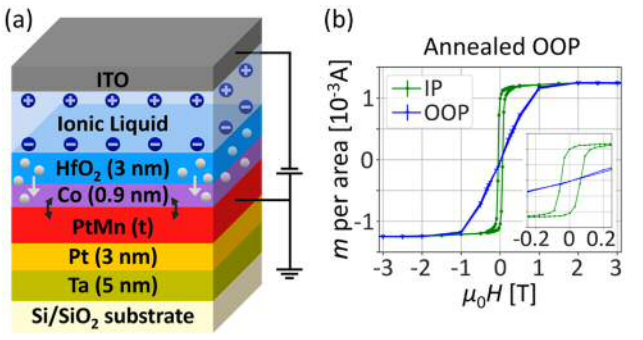

FIG. 1. (a) Sample stack. The white spheres represent the oxygen ions that can be moved by applying a gate voltage across the HfO_2. The arrow between the Co and the PtMn represents the EB coupling between the two layers. (b) SQUID measurements of the sample with 8 nm PtMn after annealing in an OOP magnetic field of 800 mT for 2 h at 300 °C. The SQUID measurements were performed along the IP (green) and OOP (blue) sample direction to confirm the fully IP magnetization of the Co. The inset shows a zoom into the center of the SQUID loops.

In the as-deposited state, the samples show full IP magnetization for both 8 and 20 nm PtMn (supplementary material Fig. S3). We aim to explore whether it is possible to reach OOP magnetization with OOP EB through ionic liquid gating. Therefore, the samples were annealed in an OOP magnetic field of 800 mT at 300 °C for 2 h, to establish OOP EB. Annealing the samples leaves the magnetization IP, while the coercivity of the IP magnetization curve increases significantly [Fig. 1(b)]. The lateral crystal orientation of PtMn (111) is not visibly affected by the annealing, as confirmed by x-ray diffraction (supplementary material Fig. S1).

The gate voltages were applied using a Keithley 2400. For each gating step, the voltage was slowly increased to minimize instabilities until reaching the desired voltage. After waiting for the desired gating time, the gate voltage was turned off and the magnetization curve was measured via the anomalous Hall effect (AHE) at room temperature. The ordinary Hall component was subtracted for each curve (see supplementary material SM2). We use the slope of the anomalous Hall resistance curve at zero remanent magnetization as a qualitative measure of the extent to which the magnetization curve is dominated by magnetic easy- or hard-axis behavior.[27]

We will first discuss the samples with the thinner PtMn layer of 8 nm. To establish a defined initial state, first, a positive gate voltage of 3.5 V was applied. This positive voltage induces an upward drag on the oxygen species inside the HfO_2 layer. The Co is set to a state of minimum oxygen concentration. As shown in Fig. 2(a), the magnetization remains IP after this initialization step, with only minor changes in the magnetization curve. Subsequently, negative voltages were applied. In agreement with previous reports,[28] we observe a progressive transformation toward a square-shaped magnetization loop. Since the AHE probes the OOP magnetization, this demonstrates that the magnetization rotates from the IP to the OOP direction. All AHE curves are shifted toward positive magnetic field values, revealing the OOP EB [Fig. 2(d)].

The OOP magnetization, which is reached by applying negative gate voltages, is very stable over time (supplementary material Fig. S5). By applying positive gate voltages, the magnetization can be rotated back toward the IP direction. However, this IP state is no longer stable over time. Within a few hours, the sample evolves back to the OOP state [Fig. 2(b)]. Additionally, it is not possible in this material system to bring the sample to an IP state by overoxidation. Instead, at −2.9 V, we observe a decrease in the total Hall resistance, while the slope continues to increase. This demonstrates the stabilization of the OOP state with EB in an initially IP sample by ionic liquid gating.

Figure 2(c) shows the evolution of the EB shift and coercivity in comparison to the slope of the AHE loop during the different gating steps. The coercivity of the AHE loops increases when the magnetization rotates from IP toward OOP. When positive voltages are applied subsequently, the magnetization direction is no longer stable in time, and the AHE curve is drifting during the measurement. The resulting

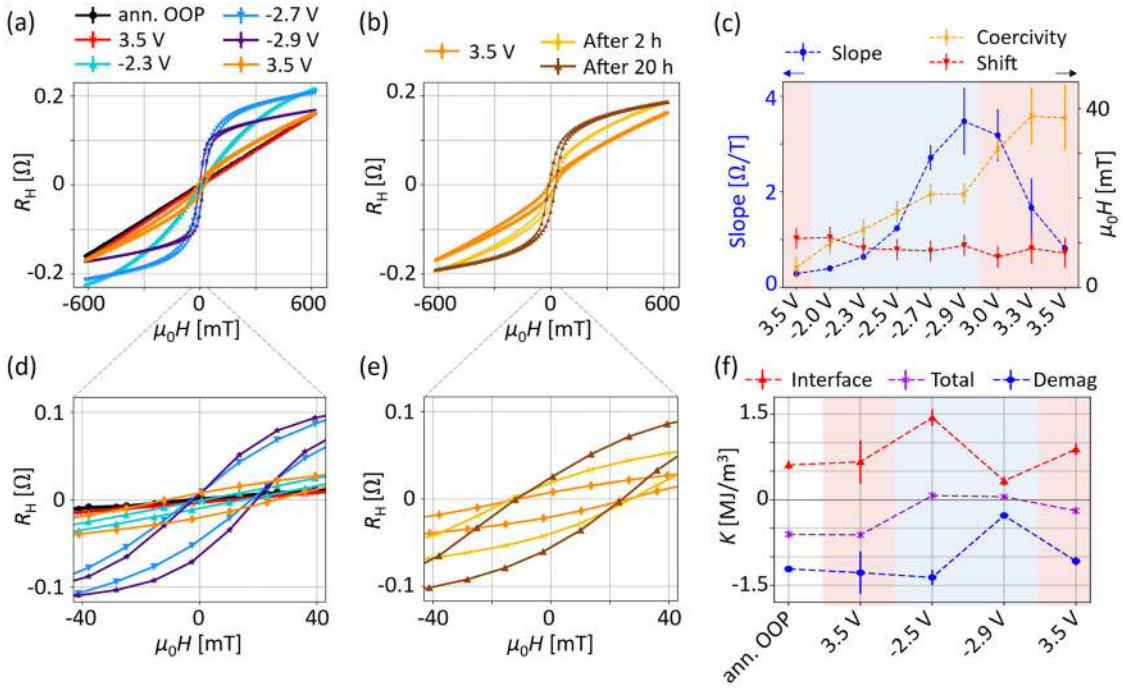

FIG. 2. Evolution of magnetic properties by gating in the sample with 8 nm PtMn. (a) AHE curves from the first gating cycle. The initialization gate voltage of 3.5 V was applied for 5 min. All further gate voltages were applied for 2 min. (b) Time evolution of the AHE curve after the magnetization was brought back toward an IP state by applying a gate voltage of 3.5 V. (c) Overview over slope, coercivity and EB shift of the AHE loops at zero remanent magnetization. (d) and (e) Zoom into subfigures (a) and (b). (f) Evolution of the total anisotropy, demagnetization, and interfacial energy per volume, obtained from SQUID measurements at 300 K (supplementary material Fig. S3). The initialization voltage of 3.5 V was applied for 10 min, all further voltages for 5 min each.

coercivities therefore have a large error. The EB shift initially decreases slightly when a negative voltage is applied. Then, it stabilizes and reaches a relatively constant value of 8.2 mT with a standard deviation of 0.8 mT and a systematical error, indicated by the error bars, of 2.4 mT (see SM7). This stabilization of the EB shift was observed in several nominally identical samples (supplementary material Fig. S8). In the annealed state, the EB shift fluctuates. However, by performing the first gating cycle, it stabilizes for all nominally identical samples to an identical value within the error margin. This indicates a varying amount of oxygen ions at the PtMn/Co interface in the annealed state, which are removed by the positive gate voltage.

To better understand the underlying magnetic changes in this system, we performed magnetization measurements in a superconducting quantum interference device (SQUID) (supplementary material Fig. S3). From the IP and OOP SQUID loops, we obtained the magnetic anisotropy energies per volume after different gating steps [Fig. 2(f)]. In this material system, we consider the demagnetization energy, which favors IP magnetization, and the interfacial anisotropy energy, which favors OOP magnetization, as the most important energy contributions. The total anisotropy energy was obtained from the area between the OOP and IP magnetization curves [Eq. (1)]. The demagnetization energy was calculated using its proportionality to the squared saturation magnetization M_S^2 [Eq. (2)].[29] The interfacial anisotropy energy, stemming from the two Co interfaces, can then be calculated using Eq. (3). The magnetization M and all anisotropies were calculated using the nominal thickness of Co.

$$K_{\text{total}} = \frac{1}{\mu_0}\int_{shift}^{\mu_0 H_{max}} (\mu_0 M_{OOP} - \mu_0 M_{IP})\, d(\mu_0 H), \tag{1}$$

$$K_{\text{demag}} = \frac{1}{2}\mu_0 M_S^2, \tag{2}$$

$$K_{\text{interface}} = K_{total} - K_{demag}. \tag{3}$$

In Fig. 2(f), the total anisotropy energy (purple) shows a clear trend of becoming more negative (toward IP magnetization) when applying positive voltages and becoming more positive (toward OOP magnetization) when applying negative voltages. This supports the presumed underlying mechanism of oxygen ion migration. The total anisotropy energy reaches its maximum positive value (maximum PMA) at −2.5 V. This is explained by the strong increase in the interfacial anisotropy (red), of a factor of 2.2, after the application of −2.5 V. This, in turn, can be explained by the additional oxygen at the Co interfaces, especially the Co/HfO_2 one. It allows for a stronger hybridization between the Co-3*d* and the O-2*p* orbitals, which is known to cause interfacial PMA.[30] Notably, the demagnetization energy (blue) remains quite constant and even slightly increases up to −2.5 V, in accordance with the observations from the AHE effect measurements. This demonstrates that the rotation of the magnetization is caused by the increasing interfacial PMA and not by a reduction of the demagnetization energy.

After the application of −2.9 V, both the demagnetization and the interfacial anisotropy energy drop significantly. For the demagnetization energy, this is clearly related to the reduction of the total

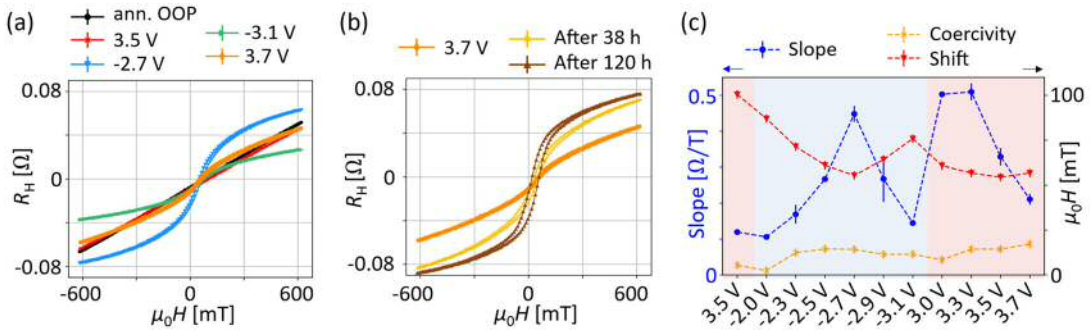

FIG. 3. Evolution of magnetic properties by gating in the sample with 20 nm PtMn. (a) AHE curves from the first gating cycle. All gate voltages were applied for 2 min. A larger version of this subfigure, which also includes the curves at −2.3 and −2.9 V can be found in SM6. (b) Time evolution of the AHE loop after the magnetization was brought back toward an IP state by applying 3.7 V. (c) Overview over slope, coercivity and EB shift of the AHE loops.

magnetic moment caused by the overoxidation of Co. The influence of overoxidation can be described as a change in the average magnetization or in the Co layer thickness, which, however, does not alter the qualitative results (supplementary material Fig. S4). For the interfacial anisotropy energy, its reduction due to overoxidation suggests that the oxygen content at the Co/HfO_2 interface has gone past the optimum oxidation point, which corresponds to maximum PMA, or that the PMA at the PtMn/Co interface got diminished. This interfacial PMA cannot be fully recovered by applying a positive voltage of 3.5 V. From the results on the AHE measurements, we can, however, assume that over time the oxygen ions will diffuse back to the positions leading to the maximum PMA.

So far, we have shown that we can establish a stable OOP magnetization with OOP EB in a sample with initial IP magnetization by ionic liquid gating. However, for applications, a much larger EB is required. Therefore, we also investigated a sample with thicker PtMn of 20 nm (Fig. 3). Similar to the stack with 8 nm PtMn, the magnetization of the sample is initially IP and remains IP after applying +3.5 V [Fig. 3(a)]. As expected, the AHE loop evolves toward a square-shaped magnetization loop by negative gating. Like in the sample with thinner PtMn, applying −2.9 V or larger negative voltages leads to overoxidation of the Co, expressed by a decrease in the total Hall resistance. However, the coercivity and the slope remain low for the applied gate voltages in the sample with thicker PtMn [Fig. 3(c)]. This changes only after performing the full first gating cycle and then waiting five days [Fig. 3(b)]. Most likely, this gives the oxygen ions time to diffuse into the energetically favored lattice positions where they can hybridize with the Co atoms, resulting in increased interfacial PMA. Presumably, this slower reorientation of the magnetization toward the OOP state, both after applying the accessible negative voltages as well as by waiting after overoxidation, is caused by a higher degree of crystallinity of Co. The Co is grown on thicker and therefore more crystalline PtMn and a higher degree of crystallinity is known to slow down oxygen diffusion.[31] This highlights the importance of the underlayer on the gating dynamics.

Just like in the thinner sample, the OOP state becomes energetically favorable as soon as it is reached once. A positive voltage initially brings the magnetization from the OOP state back toward an IP state, which, however, evolves back toward the OOP direction over time [Fig. 3(b)]. Notably, the EB shift stabilizes to a value above 50 mT in this sample, which is more than 5 times greater than in the thinner sample.

To verify whether the magnetic changes are caused by an oxidation of Co, we performed x-ray photoelectron spectroscopy (XPS) measurements. Figure 4(a) shows the XPS spectra at the Co 2p-edge in the annealed state (top) and after applying a gate voltage of −2.7 V (bottom). The annealed state shows a pure metallic Co^0 signal (blue peaks). By gating, a clear Co^{+II} signal (orange peaks) arises, confirming the partial oxidation of the Co. From SQUID measurements, we know that for the oxidized sample, around half of the magnetization is lost in the oxidized state. The strong reduction of the Co^0 peak intensity in the oxidized sample is most likely due to the surface sensitivity of XPS, indicating a stronger oxidation in the upper layers of the Co compared to the lower ones.

Understanding the oxidation of the interface between Co and PtMn is very important to retain a strong EB. Therefore, its oxidation was probed by measuring the XPS at the Mn 2p-edge [Fig. 4(b)]. Overall, the signal-to-noise ratio is worse, since the Mn atoms are lying further down below the sample surface. In the annealed state, the sample consists mainly of metallic Mn^0 (green peaks). However, after applying the negative gate voltage, also the Mn shows a clear signal of oxidation (magenta peaks). Some oxygen therefore reached the PtMn/Co interface. This is likely the reason why the EB initially drops with negative gating. However, the AHE data revealed that the EB stabilizes at a value larger than zero. This indicates that the interface does not fully get oxidized or that this oxidation does not break the exchange coupling completely. Additionally, the thinning of the Co layer by oxidation reduces the Zeeman energy and consequently leads to a relative increase in the exchange bias field. Overall, this allows for the retention of a significant EB.

In summary, we achieved the stabilization of a magnetic state with OOP magnetization and OOP EB in a sample with initial IP magnetization by ionic liquid gating. In the stack Ta (5 nm)/Pt (3 nm)/PtMn (8 nm)/Co (0.9 nm)/HfO_2 (3 nm), we showed that by applying a gate voltage of −2.7 V the magnetization could be reoriented to OOP, with an exchange bias shift of (8.2 ± 2.4) mT. SQUID and XPS measurements confirmed that the changes are due to oxygen migration in the sample. As the oxygen ions reach the Co/HfO_2 interface, the interfacial anisotropy increases, causing the reorientation of the magnetization toward the OOP direction. At large negative voltages of more

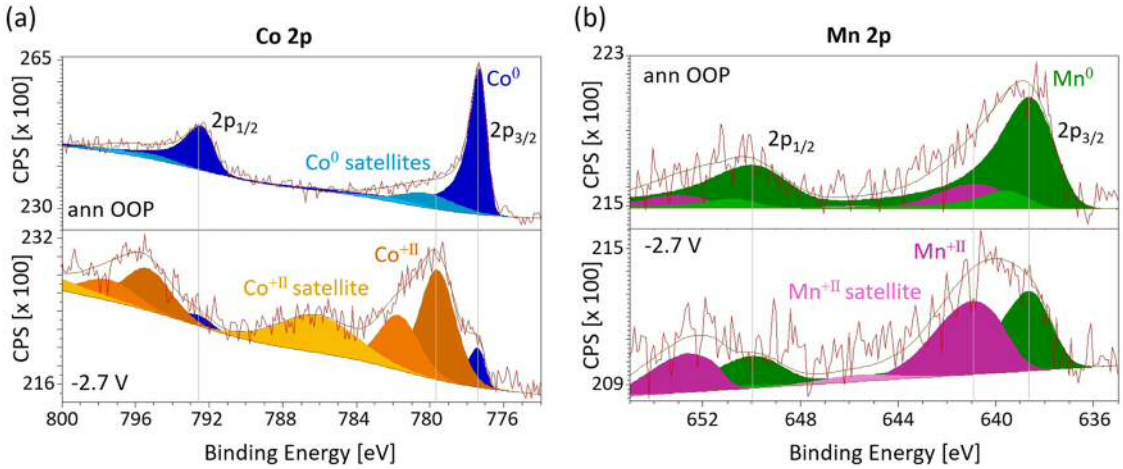

FIG. 4. XPS spectra of the sample with 8 nm PtMn, measured at (a) the Co 2p-edge and (b) the Mn 2p-edge in the states after annealing in an OOP magnetic field and after applying −2.7 V for 5 min, respectively. The Co^{+II} and Mn^{0} peaks show a multiplet splitting. Details on the experiment and the fitting procedure are given in supplementary material SM9.

than −2.7 V, both the demagnetization energy and the interfacial anisotropy energy decrease due to overoxidation of the Co. Subsequent positive voltages lead to a reorientation of the magnetization back toward the initial IP state. However, this state is volatile and evolves back toward the OOP state over time, demonstrating that the OOP state becomes the energetically favorable state once it is reached. Some of the oxygen ions also reach the bottom interface of the Co after negative gating, visible in a partial oxidation of the Mn atoms in PtMn. Notably, this oxidation does not lead to a loss of EB, just to an initial reduction of EB, which then saturates.

The sample with the thicker PtMn film of 20 nm exhibits a slower gating dynamics in the accessible voltage window, highlighting the importance of the PtMn/Co interface on the gating process. Notably, in the final state, we found fully shifted magnetization loops with a strong EB of more than 50 mT.

These results contribute to the advancement of easier and better device fabrication for energy-efficient data storage and processing as well as sensor applications.

See the supplementary material for more detailed information on measurements and data analysis.

This project has received funding from the European Union's Horizon 2020 Research and Innovation Programme under the Marie Skłodowska-Curie Grant Agreement No. 860060, "Magnetism and the effect of Electric Field" (MagnEFi), as well as from the Deutsche Forschungsgemeinschaft (DFG, German Research Foundation)—TRR 173/2-#268565370 Spin+X (Projects A01 and B02). This work was partly funded by JSPS KAKENHI Grant No. JP21H05016. We thank the Max Planck Institute for Polymer Research for access to their XPS tool.

AUTHOR DECLARATIONS

Conflict of Interest

The authors have no conflicts to disclose.

Author Contributions

Beatrice Bednarz: Conceptualization (lead); Data curation (lead); Formal analysis (lead); Investigation (lead); Methodology (equal); Project administration (lead); Visualization (lead); Writing – original draft (lead); Writing – review & editing (lead). **Maria-Andromachi Syskaki:** Data curation (supporting); Methodology (equal); Resources (equal); Validation (supporting); Writing – review & editing (equal). **Rohit Pachat:** Data curation (equal); Investigation (equal); Methodology (lead); Validation (supporting); Writing – review & editing (equal). **Leon Prädel:** Data curation (supporting); Investigation (supporting); Methodology (supporting); Resources (equal); Validation (supporting). **Martin Wortmann:** Formal analysis (supporting); Validation (equal); Writing – review & editing (equal). **Timo Kuschel:** Formal analysis (supporting); Validation (equal); Writing – review & editing (equal). **Shimpei Ono:** Methodology (supporting). **Mathias Kläui:** Funding acquisition (equal); Resources (equal); Supervision (equal); Validation (equal); Writing – review & editing (equal). **Liza Herrera Diez:** Conceptualization (equal); Funding acquisition (lead); Methodology (lead); Resources (equal); Supervision (supporting); Validation (supporting); Writing – review & editing (equal). **Gerhard Jakob:** Data curation (supporting); Formal analysis (equal); Funding acquisition (lead); Investigation (supporting); Project administration (equal); Resources (lead); Supervision (lead); Validation (lead); Writing – review & editing (lead).

DATA AVAILABILITY

Data that support the findings of this study are openly available in Zenodo at https://doi.org/10.5281/zenodo.11395888 (Ref. 32).

REFERENCES

[1]International Energy Agency, see https://www.iea.org/reports/digitalisation-and-energy for "Digitalization and energy" (2017).
[2]L. Belkhir and A. Elmeligi, "Assessing ICT global emissions footprint: Trends to 2040 & recommendations," J. Clean. Prod. **177**, 448–463 (2018).

[3]M. Weisheit, S. Fähler, A. Marty, Y. Souche, C. Poinsignon, and D. Givord, "Electric field-induced modification of magnetism in thin-film ferromagnets," Science **315**(5810), 349–351 (2007).
[4]F. Matsukura, Y. Tokura, and H. Ohno, "Control of magnetism by electric fields," Nat. Nanotechnol. **10**(3), 209–220 (2015).
[5]C. Song, B. Cui, F. Li, X. Zhou, and F. Pan, "Recent progress in voltage control of magnetism: Materials, mechanisms, and performance," Prog. Mater. Sci. **87**, 33–82 (2017).
[6]A. Molinari, H. Hahn, and R. Kruk, "Voltage-control of magnetism in all-solid-state and solid/liquid magnetoelectric composites," Adv. Mater. **31**(26), 1806662 (2019).
[7]J. Grollier, D. Querlioz, K. Y. Camsari, K. Everschor-Sitte, S. Fukami, and M. D. Stiles, "Neuromorphic spintronics," Nat. Electron. **3**(7), 360–370 (2020).
[8]B. Dieny, I. L. Prejbeanu, K. Garello, P. Gambardella, P. Freitas, R. Lehndorff, W. Raberg, U. Ebels, S. O. Demokritov, J. Akerman, A. Deac, P. Pirro, C. Adelmann, A. Anane, A. V. Chumak, A. Hirohata, S. Mangin, S. O. Valenzuela, M. C. Onbaşlı, M. d'Aquino, G. Prenat, G. Finocchio, L. Lopez-Diaz, R. Chantrell, O. Chubykalo-Fesenko, and P. Bortolotti, "Opportunities and challenges for spintronics in the microelectronics industry," Nat. Electron. **3**(8), 446–459 (2020).
[9]M. Ameziane, R. Mansell, V. Havu, P. Rinke, and S. van Dijken, "Lithium-ion battery technology for voltage control of perpendicular magnetization," Adv. Funct. Mater. **32**(29), 2113118 (2022).
[10]U. Bauer, L. Yao, A. J. Tan, P. Agrawal, S. Emori, H. L. Tuller, S. van Dijken, and G. S. D. Beach, "Magneto-ionic control of interfacial magnetism," Nat. Mater. **14**(2), 174–181 (2015).
[11]J. Zehner, D. Wolf, M. U. Hasan, M. Huang, D. Bono, K. Nielsch, K. Leistner, and G. S. D. Beach, "Magnetoionic control of perpendicular exchange bias," Phys. Rev. Mater. **5**(6), L061401 (2021).
[12]M. U. Hasan, A. E. Kossak, and G. S. D. Beach, "Large exchange bias enhancement and control of ferromagnetic energy landscape by solid-state hydrogen gating," Nat. Commun. **14**(1), 8510 (2023).
[13]L. Herrera Diez, Y. T. Liu, D. A. Gilbert, M. Belmeguenai, J. Vogel, S. Pizzini, E. Martinez, A. Lamperti, J. B. Mohammedi, A. Laborieux, Y. Roussigné, A. J. Grutter, E. Arenholtz, P. Quarterman, B. Maranville, S. Ono, M. S. E. Hadri, R. Tolley, E. E. Fullerton, L. Sanchez-Tejerina, A. Stashkevich, S. M. Chérif, A. D. Kent, D. Querlioz, J. Langer, B. Ocker, and D. Ravelosona, "Nonvolatile ionic modification of the Dzyaloshinskii-Moriya interaction," Phys. Rev. Appl. **12**(3), 034005 (2019).
[14]J. Zehner, I. Soldatov, S. Schneider, R. Heller, N. B. Khojasteh, S. Schiemenz, S. Fähler, K. Nielsch, R. Schäfer, and K. Leistner, "Voltage-controlled deblocking of magnetization reversal in thin films by tunable domain wall interactions and pinning sites," Adv. Electron. Mater. **6**(11), 2000406 (2020).
[15]C. Balan, J. Peña Garcia, A. Fassatoui, J. Vogel, D. de, S. Chaves, M. Bonfim, J.-P. Rueff, L. Ranno, and S. Pizzini, "Tuning the dynamics of chiral domain walls of ferrimagnetic films by magnetoionic effects," Phys. Rev. Appl. **18**(3), 034065 (2022).
[16]J. Nogués and I. K. Schuller, "Exchange bias," J. Magn. Magn. Mater. **192**(2), 203–232 (1999).
[17]A. van den Brink, G. Vermijs, A. Solignac, J. Koo, J. T. Kohlhepp, H. J. M. Swagten, and B. Koopmans, "Field-free magnetization reversal by spin-Hall effect and exchange bias," Nat. Commun. **7**(1), 10854 (2016).
[18]A. Ehresmann, D. Lengemann, T. Weis, A. Albrecht, J. Langfahl-Klabes, F. Göllner, and D. Engel, "Asymmetric magnetization reversal of stripe-patterned exchange bias layer systems for controlled magnetic particle transport," Adv. Mater. **23**(46), 5568–5573 (2011).
[19]Y. Wang, X. Zhou, C. Song, Y. Yan, S. Zhou, G. Wang, C. Chen, F. Zeng, and F. Pan, "Electrical control of the exchange spring in antiferromagnetic metals," Adv. Mater. **27**(20), 3196–3201 (2015).
[20]M. Wang, M. Li, Y. Lu, X. Xu, and Y. Jiang, "Electric field controlled perpendicular exchange bias in Ta/Pt/Co/IrMn/Pt heterostructure," Appl. Phys. Lett. **123**(12), 122405 (2023).
[21]J. Zehner, R. Huhnstock, S. Oswald, U. Wolff, I. Soldatov, A. Ehresmann, K. Nielsch, D. Holzinger, and K. Leistner, "Nonvolatile electric control of exchange bias by a redox transformation of the ferromagnetic layer," Adv. Electron. Mater. **5**(6), 1900296 (2019).
[22]Z. Mustafa, D. Pravarthana, B. Wang, H. Yang, and R.-W. Li, "Manipulation of exchange bias effect via all-solid-state Li-ion redox capacitor with antiferromagnetic electrode," Phys. Rev. Appl. **14**(1), 014062 (2020).
[23]C. J. Jensen, A. Quintana, P. Quarterman, A. J. Grutter, P. P. Balakrishnan, H. Zhang, A. V. Davydov, X. Zhang, and K. Liu, "Nitrogen-based magneto-ionic manipulation of exchange bias in CoFe/MnN heterostructures," ACS Nano **17**(7), 6745–6753 (2023).
[24]G. W. Anderson, Y. Huai, and M. Pakala, "Spin-valve thermal stability: The effect of different antiferromagnets," J. Appl. Phys. **87**(9), 5726–5728 (2000).
[25]Y. K. Kim, S.-R. Lee, S. A. Song, G.-S. Park, H. S. Yang, and K.-I. Min, "Magnetoresistance and interlayer diffusion in PtMn spin valves upon postdeposition annealing," J. Appl. Phys. **89**(11), 6907–6909 (2001).
[26]A. B. Mukhopadhyay, C. B. Musgrave, and J. Fdez. Sanz, "Atomic layer deposition of hafnium oxide from hafnium chloride and water," J. Am. Chem. Soc. **130**(36), 11996–12006 (2008).
[27]B. Dieny and M. Chshiev, "Perpendicular magnetic anisotropy at transition metal/oxide interfaces and applications," Rev. Mod. Phys. **89**(2), 025008 (2017).
[28]R. Pachat, D. Ourdani, J. W. van der Jagt, M.-A. Syskaki, A. Di Pietro, Y. Roussigné, S. Ono, M. S. Gabor, M. Chérif, G. Durin, J. Langer, M. Belmeguenai, D. Ravelosona, and L. H. Diez, "Multiple magnetoionic regimes in Ta/$Co_{20}Fe_{60}B$/HfO_2," Phys. Rev. Appl. **15**(6), 064055 (2021).
[29]S. Blundell, *Magnetism in Condensed Matter* (OUP Oxford, 2001).
[30]H. X. Yang, M. Chshiev, B. Dieny, J. H. Lee, A. Manchon, and K. H. Shin, "First-principles investigation of the very large perpendicular magnetic anisotropy at Fe|MgO and Co|MgO interfaces," Phys. Rev. B **84**(5), 054401 (2011).
[31]R. Pachat, D. Ourdani, M.-A. Syskaki, A. Lamperti, S. Roy, S. Chen, A. D. Pietro, L. Largeau, R. Juge, M. Massouras, C. Balan, J. W. van der Jagt, G. Agnus, Y. Roussigné, M. Gabor, S. M. Chérif, G. Durin, S. Ono, J. Langer, D. Querlioz, D. Ravelosona, M. Belmeguenai, and L. Herrera Diez, "Magneto-ionics in annealed W/CoFeB/HfO_2 thin films," Adv. Mater. Interfaces **9**(36), 2200690 (2022).
[32]B. Bednarz, M.-A. Syskaki, R. Pachat, L. Prädel, M. Wortmann, T. Kuschel, S. Ono, M. Kläui, L. Herrera Diez, and G. Jakob (2024). "Stabilizing perpendicular magnetic anisotropy with strong exchange bias in PtMn/Co by magneto-ionics," Dataset, Zenodo. https://doi.org/10.5281/zenodo.11395888